From Squaric Acid Amides (SQAs) to Quinoxaline-Based SQAs—Evolution of a Redox-Active Cathode Material for Organic Polymer Batteries

Marcel E. Baumert, Victoria Le, Po-Hua Su, Yosuke Akae, Dominic Bresser,* Patrick Théato,* and Max M. Hansmann*

ABSTRACT: The search for new redox-active organic materials (ROMs) is essential for the development of sustainable energy-storage solutions. I n this study, we present a new class of cyclobuta[*b*]quinoxaline-1,2-diones or squaric acid quinoxalines (SQXs) as highly promising candidates for ROMs featuring exceptional stability and high redox potentials. While simple 1,2- and 1,3-squaric acid amides (SQAs), initially reported by Hünig and coworkers decades ago, turned out to exhibit low stability in their radical cation oxidation states, we demonstrate that embedding the nitrogen atoms into a quinoxaline heterocycle leads to robust two-electron SQX redox systems. A series of SQX compounds, as well as their corresponding radical cations, were prepared and fully characterized, including EPR spectroscopy, UV–vis spectroscopy, and X-ray diffraction. Based on the promising electrochemical properties and high stability of the new ROM, we developed SQX-functionalized polymers and investigated their physical and electrochemical properties for energy-storage applications. These polymers showed remarkable thermal stability well above 200 °C with reversible redox properties and potentials of about 3.6 V vs Li^+/Li. By testing the galvanostatic cycling performance in half-cells with lithium-metal counter electrodes, a styrene-based polymer with SQX redox side groups showed stable cycling for single-electron oxidation for more than 100 cycles. These findings render this new class of redox-active polymers as highly promising materials for future energy-storage applications.

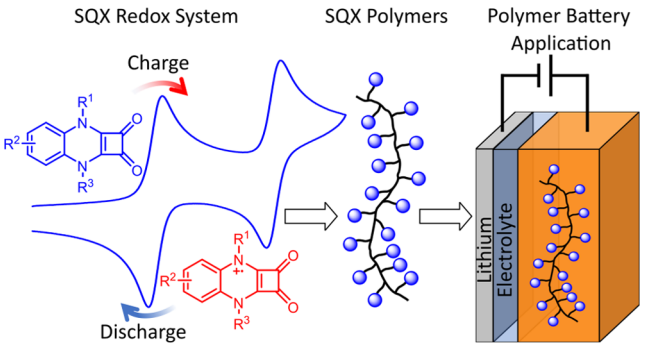

INTRODUCTION

The rapidly growing demand for sustainable energy-storage solutions is a global economic and scientific challenge. The currently dominating electrochemical energy-storage technology, lithium-ion batteries (LIBs), are based on metal-containing electrodes, which are usually difficult to recycle and still rather expensive.[1,2] Additionally, a major concern is the unstable supply of key resources, namely cobalt, nickel, and lithium, due to their natural geographical concentration and distribution.[3] A solution for low-cost, sustainable, and high-performance batteries can be metal-free batteries based on redox-active organic materials (ROMs),[4,5] especially in the context of redox polymer-derived organic batteries.[6−9] Since ROMs are composed of inexpensive, light, and abundant elements, like carbon, nitrogen, hydrogen, oxygen, and sulfur, ROM-based batteries might not only be more cost-effective than LIBs but also open the avenue to sustainability.[10−14] One main challenge to developing organic batteries relies on the identification of stable organic cathode materials, which retain high stability over repetitive cycling and, at the same time, feature a high energy density.[15] Well-defined redox active moieties for cathode materials are, for instance, phenazine such as DMPZ,[16] nitroxide radicals such as TEMPO,[17−19] phenothiazines[20,21] such as MEEPT,[20] cyclopropenium salts (CP),[22−25] or dimethoxybenzenes (Scheme 1).[26−29] Embedding small redox active molecules into polymeric frameworks disfavors migration processes between the electrodes and enables an easier material processing.[20] Among the most prominent and thoroughly investigated ROMs are polymeric nitroxide radicals such as poly(2,2,6,6-tetramethyl-1-piperidinyloxy methacrylate) (PTMA)[30−32] or poly(galvinoxyl-styrene).[15,33] However, other ROMs have also been successfully turned into polymer cathode materials such as phenazines,[34−36] phenothiazines/oxazines,[37−39] dimethoxybenzenes,[40] and cyclopropenium salts.[41]

Scheme 1. Well Investigated Monomeric (Top) and Polymeric (Bottom) ROMs as Positive Electrode Active Materials with Their Respective Oxidation Potentials

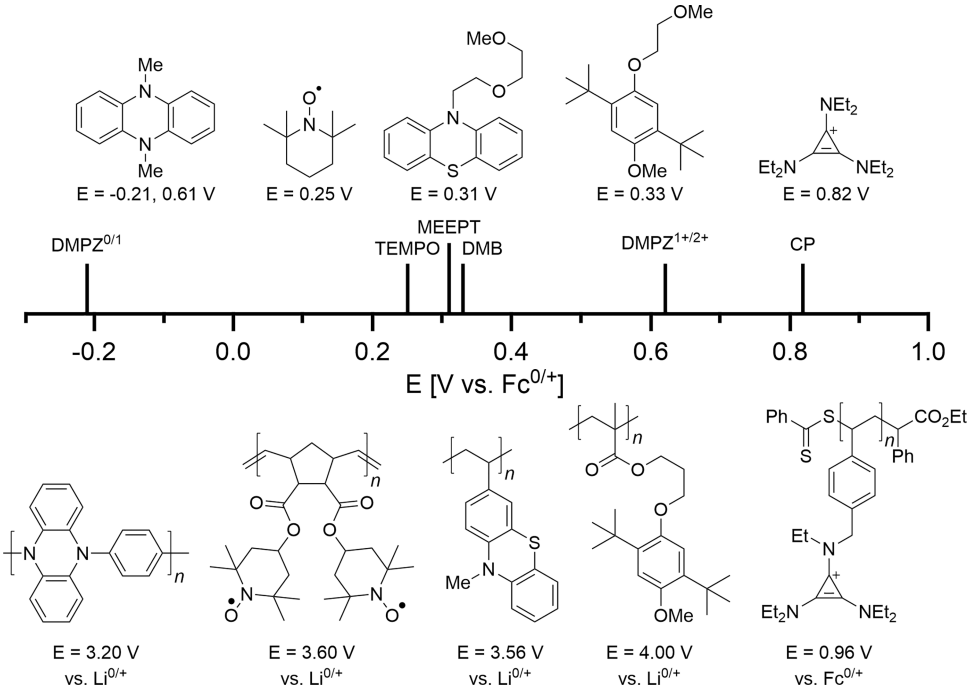

We were interested in exploring novel ROM architectures as cathode materials, ideally with enhanced stability and increased redox potential compared to the *de facto* gold standard PTMA. In search of alternative redox-active moieties, we were particularly interested in squaric acid amides (SQAs) due to their low molecular mass and straightforward synthetic access. The four-membered SQA ring system is characterized by very high thermal stability and has found many applications, for instance, in organocatalysis,[42] anion sensing,[43] or as pharmacophores in medicinal chemistry.[44] Surprisingly, the redox properties of SQAs, even though already reported in 1977 by Hünig and coworkers,[45−47] did not attract any attention in the field of energy storage over the last decades. Since the isolation and stability of the radical cations obtained upon oxidation of SQAs were not reported, it was aimed at (i) systematically investigating and optimizing the SQA building block with a focus on maximizing the stability of the radical cation oxidation state, decreasing the solubility, and increasing the redox-potential. With the most promising ROMs in hand, we aimed at (ii) designing the corresponding monomers and their polymerization to (iii) yield a first proof-of-concept polymer cathode containing squaric acid amides as a novel ROM.

RESULTS AND DISCUSSION

Squaric Acid Amide (SQA) Redox System. We started our investigation by the synthesis of a series of 1,2- and 1,3-substituted SQA redox systems by condensing secondary amines with commercially available squaric acid ester (**1a**) or squaric acid (**1b**) (Scheme 2). The reaction with the ester **1a** afforded in high yields the stable 1,2-SQA molecules, which feature alkyl/aryl amines (**2a**), cyclic amines (**2b**), or alkyl bridged diamines with $(CH_2)_n$ (n = 2, 3) linkers (**2c−d**).[48] The reaction with squaric acid afforded 1,3-SQA **4a**. **4b** was accessed by transamination from **4a**.[49] The isomeric 1,2-SQA **2b** and 1,3-SQA **4b** featuring piperidyl substituents could be unambiguously structurally verified by X-ray crystallography (Figures S124 and S125). Besides the SQA system, the synthesis of semi-squaric acid amides (SSQA)[50] featuring C−aryl (**6a−6b**; **6d**), C−alkyl (**6c**), as well as C−OEt (**6e**) moieties was also investigated (Scheme 2; for synthetic details, see SI).

Subsequently, the different SQA and SSQA molecules were investigated by cyclic voltammetry (CV). In agreement with the report by Hünig and coworkers,[45] all investigated 1,2 and 1,3-SQA molecules featured a reversible single-electron oxidation and an irreversible second oxidation[51] (for the redox potentials, see Scheme 2 and SI). Exemplary, **2a** featured a reversible oxidation event at $E_{1/2}$ = 0.67 V vs the ferrocene redox couple ($Fc^{0/+}$) in MeCN (1.06 V vs SCE) to afford the radical cation **3a** (Figure 1A). The 1,3-isomer SQA **4a** featured a reversible redox event at a slightly lower oxidation potential $E_{1/2}$ = 0.61 V vs $Fc^{0/+}$ in MeCN to yield the radical cation **5a** (Figure S19). The semi-squaric acids **6a−6d** featured irreversible redox events at strongly positive potentials [1.34 V (**6a**), 1.22 V (**6b**), 1.37 V (**6c**) and 1.20 (**6d**) vs $Fc^{0/+}$ (Figures S25−S38)], while **6e** featured a reversible oxidation event at 1.02 V (Figure S39). Due to the irreversible oxidation event of SSQAs **6a−6d**, these molecules were not further considered suitable energy-storage materials.

Based on the promising CV data, stoichiometric chemical oxidation was investigated. 1,2-SQAs (**2a−2d**) and 1,3-SAQs (**4a−4b**) were oxidized by $NOSbF_6$ to afford radical cations **3a−3d** and **5a−5b** as SbF_6^- salts, respectively. For **6e**, electrochemically reversible oxidation at 1.02 V vs $Fc^{0/+}$ was observed. However, the oxidation with $NOSbF_6$ and $SbCl_5$ did not yield a radical cation, and therefore, **6e** was not further considered. The formation of **3a** was monitored by performing a UV−vis spectroelectrochemical measurement (Figure 1B), which matched the UV−vis spectrum of isolated radical cation **3a**. Interestingly, the radical cation **3a** featured strong vis and NIR absorptions at λ = 637 and 952 nm, which might be

Scheme 2. Synthesis and Reversible Oxidation of SQA Containing the 1,2-SQA and 1,3-SQA Cores (Top) as well as Semi-Squaric Acid Amides SSQAs 6a–6d and 6e (Bottom)[a]

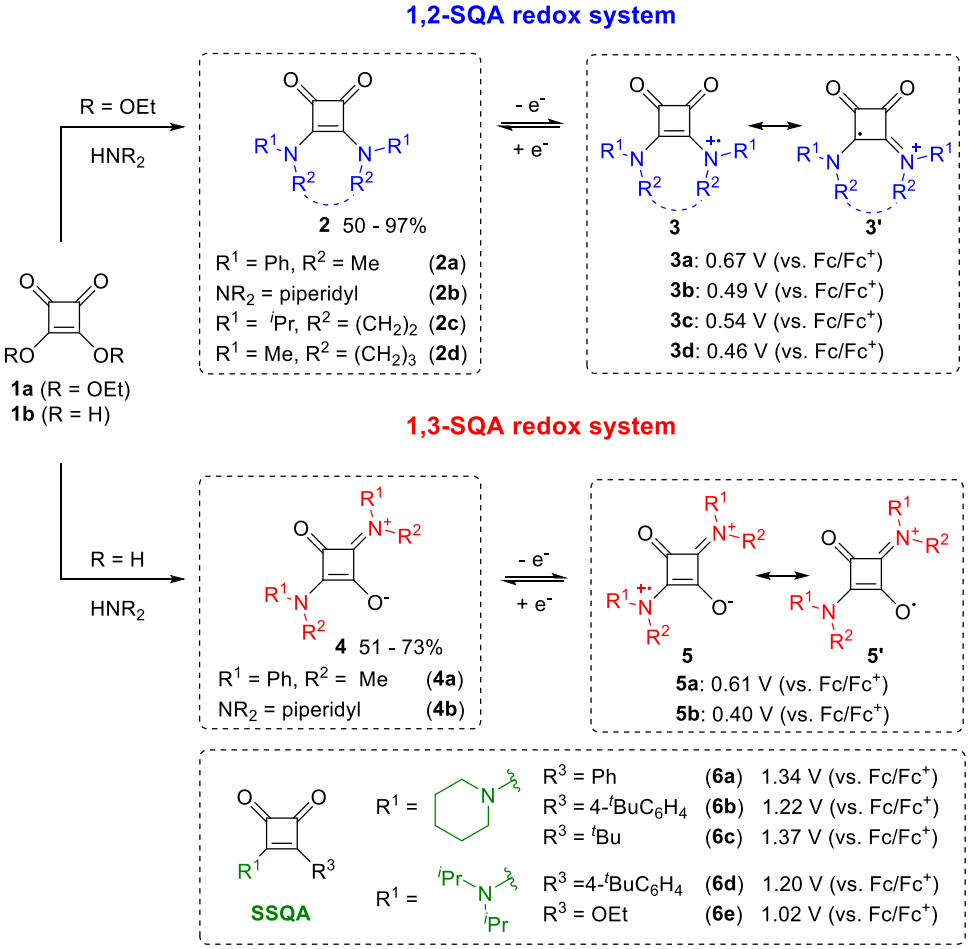

[a]Redox potentials are determined by CV and referenced against $Fc^{0/+}$.

attributed to an intervalence charge transfer (IVCT) band, presumably through intermolecular radical cation/radical cation interactions such as $\pi-\pi$ stacking.[52] The open-shell nature of **3a–3d** and **5a–5b** was unambiguously identified by EPR spectroscopy (for **3a** see Figure 1C; for all others, see Figures S256–S262). The fitted EPR data agreed well with the computationally predicted EPR hyperfine coupling parameters of the DFT-optimized radical cations.

We next monitored the time-dependent UV–vis absorption to evaluate the stability of radical cation **3a** under inert conditions. While the UV–vis absorption decayed very slowly at −40 °C (Figure S4), importantly, a significant decomposition of **3a** on the time scale of minutes/hours at room temperature ($t_{1/2}$ ~ 300 min; Figure 1D) could be observed. Clearly, even though the oxidation event appeared reversible on the CV time scale (Figure 1A), the radical stability appeared to be very poor in solution. Unfortunately, this observation was not restricted to the N(Me)Ph substitution pattern of **3a** but turned out to be a general observation also for the other 1,2-SQAs (**3a–3d**) ($t_{1/2}$ (**3a**) ~ 300 min; $t_{1/2}$ (**3b**) ~ 120 min; $t_{1/2}$ (**3c**) ~ 130 min) as well as 1,3-SQAs (**5a–5b**) ($t_{1/2}$ (**5a**) ~ 300 min; $t_{1/2}$ (**5b**) ~ 420 min) systems (Figure 1E). The low stability of the SQA radical cations rendered them not attractive candidates for energy-storage applications and motivated us to re-evaluate the structure of the SQA system.

Evolution of the Squaric Acid Amide Building Block—The SQX Redox System—A Stable Two-Electron Redox System. Due to the poor stability of the radical cation oxidation state of the SQA systems, we aimed to increase the stability of the open-shell system by increasing its π-delocalization and thereby embedding the two amino groups into an aromatic quinoxaline heterocycle. Such cyclobuta[*b*]-quinoxaline-1,2-diones or squaric acid quinoxalines (SQXs) can be considered as a hybrid of the well-known phenazine core and squaric acid amides (Scheme 3A). Notably, only a single alkyl SQX example (R = N–Me) was reported previously by Hünig and coworkers in 1977 and the compound class remained unnoticed without applications in the chemical literature.[45,46,53]

A simple two-step protocol was developed consisting of amide formation followed by alkylation or arylation to give access to a large array of structurally modified SQX molecules in generally high yields (Scheme 3B). Straightforward condensation of commercially available squaric acid (**1b**) with 1,2-diaminobenzenes (**7**) affords the SQX core (**8a–8d**).[53] Alkylation led to symmetrical compounds **9a–9c**. After screening a series of unsuccessful Buchwald–Hartwig C–N coupling conditions for *N*-arylation, we were delighted to

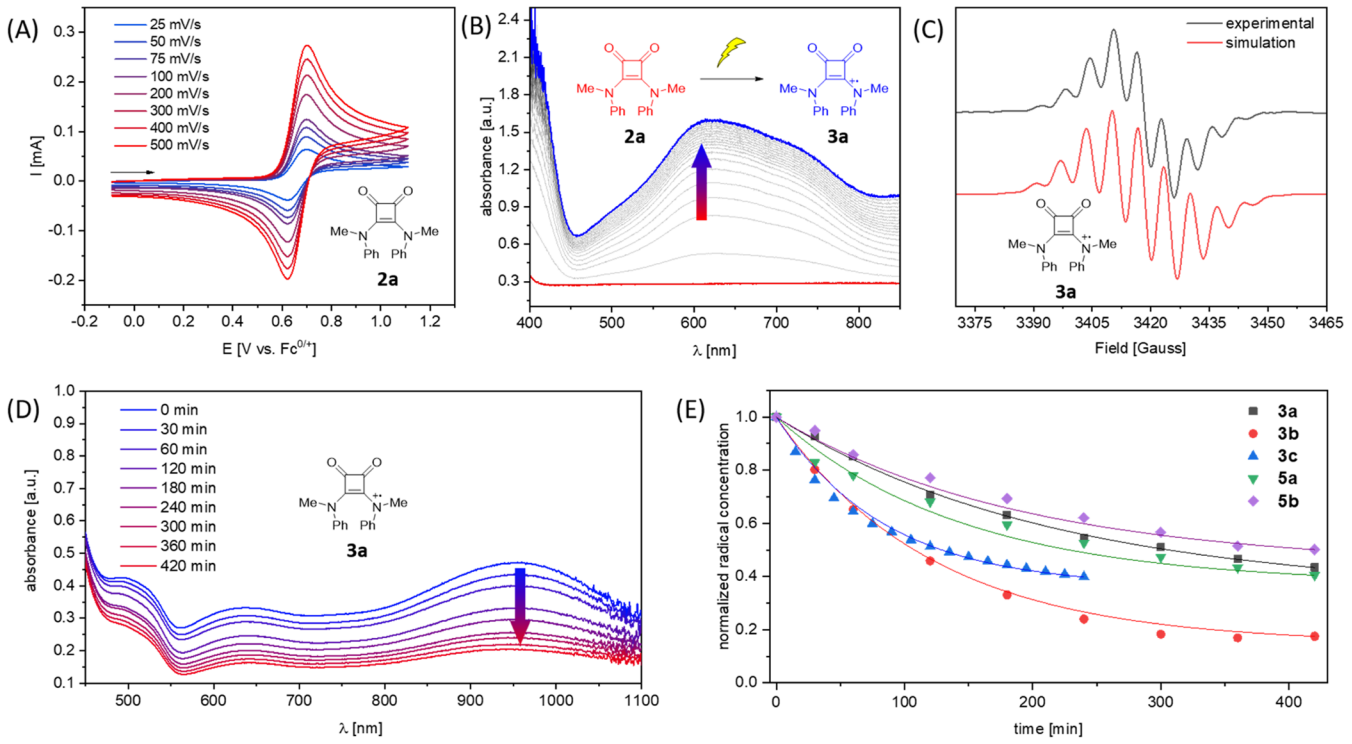

Figure 1. (A) Cyclic voltammograms for **2a** in MeCN (0.1 M nBu$_4$PF$_6$) and (B) X-band EPR spectrum of radical **3a**; fitted (calculated) EPR parameter in [MHz]: 2xN = 19.2 (20.0), 6xH = 17.0 (19.3). (C) Spectroelectrochemistry for the oxidation of **2a** to **3a**; (D) decay of the UV−vis absorption for isolated radical **3a**; and (E) time-dependent stability measurements (UV−vis) of the radicals **3a**−**3c**, **5a**, and **5b** in MeCN at room temperature.

observe that *N*-arylation proceeded in good yields (81%), employing hypervalent iodonium salt $Ph_2I^+PF_6^-$ in the presence of a copper catalyst to afford the unknown arylated SQX *N*−Ph/*N*−Ph derivative **9d**. We also investigated the substitution of the quinoxaline core by the installation of donor groups (**9f**−**9g**) and brominated substituents (**9h**−**9i**, **9k**). The later halogenated substitutions (**9i**, **9k**) allowed further possibilities for functionalization by Suzuki−Miyaura cross-coupling, such as **9j** and **9l**. Additionally, higher stabilities were expected for the halogenated radicals in analogy to the triarylamine redox system magic-blue.[54]

With a library of 12 bench-stable SQX molecules in hand, we next investigated the electrochemical behavior by CV (Figures 2 and S42−S82). In all cases, except for **9k** and **9l**, a reversible two-step oxidation process was observed to give radical cation **10** and dication **11**. Additionally, the SQX systems also showed an irreversible reduction event at strongly negative potentials (−2.37 to −2.54 V), which was due to its irreversibility not further considered (see Figure S83). In contrast, the oxidation to the dicationic oxidation state of the SQX systems was compared to that of the SQA system (*vide supra*), typically reversible. The parent system (*N*−Me) **9a** featured a first oxidation at $E^1_{1/2}$ = 0.32 V (vs $Fc^{0/+}$) ca. 300 mV lower in potential than the oxidation of SQAs **2a** or **4a** and a second reversible oxidation at a remarkably high positive potential of $E^2_{1/2}$ = 1.13 V (vs $Fc^{0/+}$) (Figure 2). Switching from *N*−Me (**9a**) to *N*−Ph (**9d**) increased the oxidation potential for both redox events by ca. 150 mV, while a similar trend was observed for electronegative substitution on the quinoxaline core (**9i**). Importantly, the redox potential can be tuned strongly by the installation of two donor (OMe) groups on the quinoxaline core (**9f**), allowing the second oxidation event to be shifted to $E^2_{1/2}$ = 0.72 V.

For **9f**, the electrochemical oxidation was monitored by UV−vis spectroelectrochemistry, confirming the formation of the two well-defined redox states, the radical cation **10f** and dication **11f** at the given redox potentials (Figure 3A). TD-DFT calculations were performed at the B3LYP/def2tzvpp//B3LYP-D3BJ/def2svp level of theory and show good accordance with the experimentally recorded UV−vis for the neutral compound **9f**, the radical cation **10f**, as well as the electrochemically generated dication **11f** (Figures S292−294). Subsequently, oxidation of all SQX molecules **9a**−**9l** by stoichiometric amounts of one equivalent of oxidant $NOSbF_6$ allowed for the clean isolation of the radical cations **10a**−**10l** in quantitative yields. In the case of neutral SQX **9e** as well as the radical cations **10e** and **10i**, it was possible to obtain single crystals suitable for X-ray solid-state structure determination (Figures 3B and S121−S123). These X-ray structures represent the first solid-state structures of the SQX system and any squaric acid amide-derived radical cations.[55] Interestingly, the C2−C3 bond is unusually long for a C(sp^2)−C(sp^2) bond in neutral **9e** [C2−C3 1.531(2) Å] (typically ca. 1.46−1.54 Å) and significantly further elongated in the radical cations [1.570(2) Å (**10e**) and 1.562(3) Å (**10i**)] (for a comparison of the bond parameter of squaric acid amides based upon a search within the Cambridge Crystallographic Database, see Figure S126).

Additionally, all radical cations **10a**−**10l** were clearly identified by EPR spectroscopy (**10a** and **10l** Figure 3C; for additional EPR spectra, see Figures S262−S273). The fitted EPR spectra agree very well with the DFT-calculated hyperfine coupling constants, clearly indicating a high degree of spin

Scheme 3. (A) Merging the SQA and Phenazine Cores to Afford SQX Redox Systems; (B) SQX Redox System with Their Corresponding Oxidation States and Redox Potentials (vs $Fc^{0/+}$)[a]

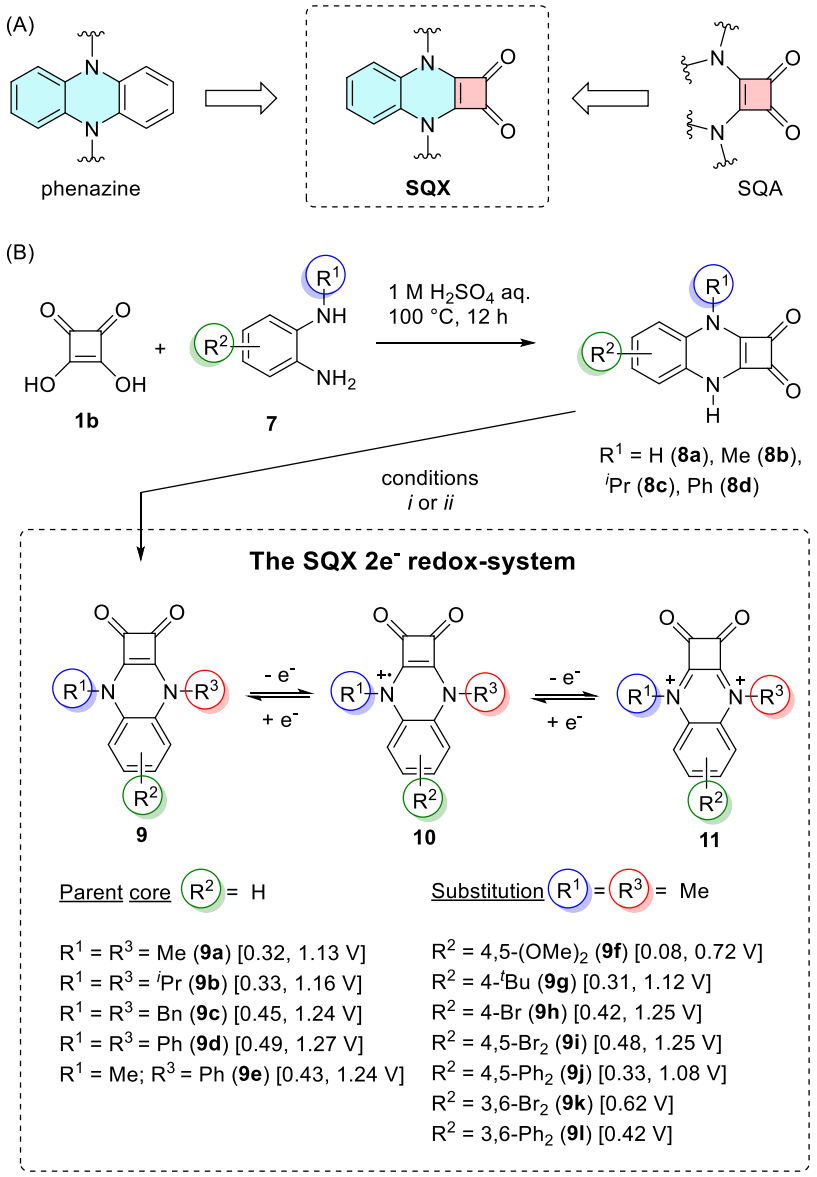

[a](i) (alkylation): K_2CO_3 (3.0 equiv), R^3X (3.0 equiv), DMF, rt, 12 h; (ii) (arylation): K_2CO_3 (1.5 equiv), CuI (20 mol %), $Ph_2I^+PF_6^-$ (1.5 equiv), DMF, 40 °C, 12 h.

density on nitrogen (a_N = 18.2 MHz (**10a**)) similar to the SQA systems [a_N = 19.2 MHz (**3a**)].[56]

Next, the stability of the SQX radical cations **10** was investigated by time-dependent UV−vis spectroscopy under inert conditions. Importantly, all investigated SQX radical cations were remarkably stable with a decay of ca. 10−20% over 2 weeks (Figure 3D). Note, in comparison, the SQA-derived molecules decomposed strongly over the course of a few hours (see above). In fact, the radical cation **10a** could be detected over days/weeks in solution (Figure S5). Even under aerobic conditions using nondry MeCN, the radical remained stable without any significant decomposition for at least 10 days. For **10j**, we even observed an EPR signal after 8 months, demonstrating the excellent stability of the radical cation oxidation state.

In the case of **9a** and **9d**, we also attempted the synthesis of the dicationic oxidation states. However, it was difficult to find the right stoichiometric oxidant for such high oxidation potentials with E > 1 V (including $SbCl_5$). Electrochemical oxidation caused separation problems associated with the electrolyte salt. We also noted that the dicationic *N*-alkyl-substituted SQX systems are prone to dealkylation reactions, thereby increasing the difficulty in their clean isolation.

To further confirm the high stability of the radical cations and to evaluate the electrochemical cycling stability, charge/discharge studies in a symmetrical H-cell were performed (Figure 4).

The symmetrical H-cell was loaded with 5.0 mM solutions of **9j** and **10j** in MeCN, and galvanostatic cycling (3.2 mA/2C; cutoff potentials at E = 0.8 and 0.0 V vs $Ag/AgNO_3$) with reticulated vitreous carbon electrodes was performed (for details, see SI). In agreement with the high radical stability determined by UV−vis measurements, the redox system **9j**/**10j** remained stable over 150 dis-/charge cycles with

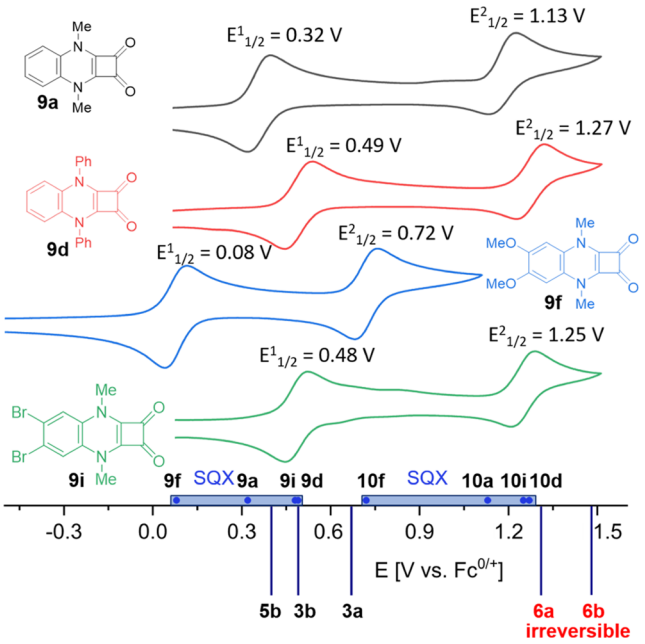

Figure 2. Comparison of representative CVs for selected SQX systems in MeCN (0.1 M nBu$_4$PF$_6$) at a scan rate of 200 mV s^{-1}.

essentially perfect Coulombic efficiency and only ca. 10% capacity loss (Figure 4). The time-dependent dis-/charge

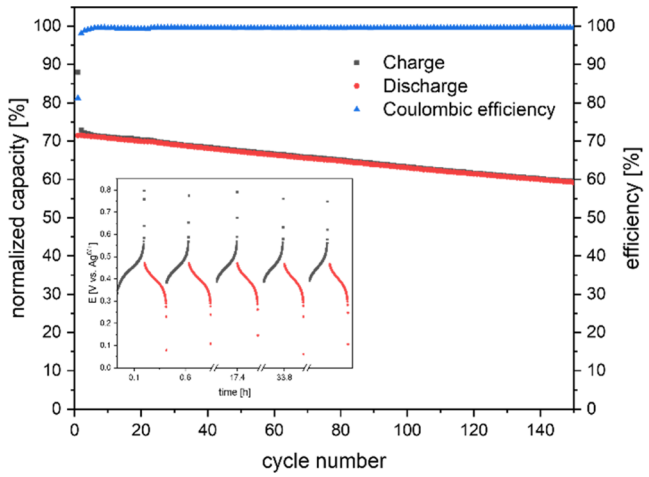

Figure 4. Cyclic charge−discharge studies of redox system **9j**/**10j**; inset: charge−discharge profile for the cycling experiments.

profiles (inset of Figure 4) showed a stable (sloped) plateau over the 150 cycles, thus further confirming the promising redox stability, especially of the *N*-alkyl systems (for galvanostatic dis-/charge studies of **9b**/**10b** and **9e**/**10e**, see Figures S93−S96).

Redox-Active Polymer Synthesis and Characterization. The highly promising stability and electrochemical

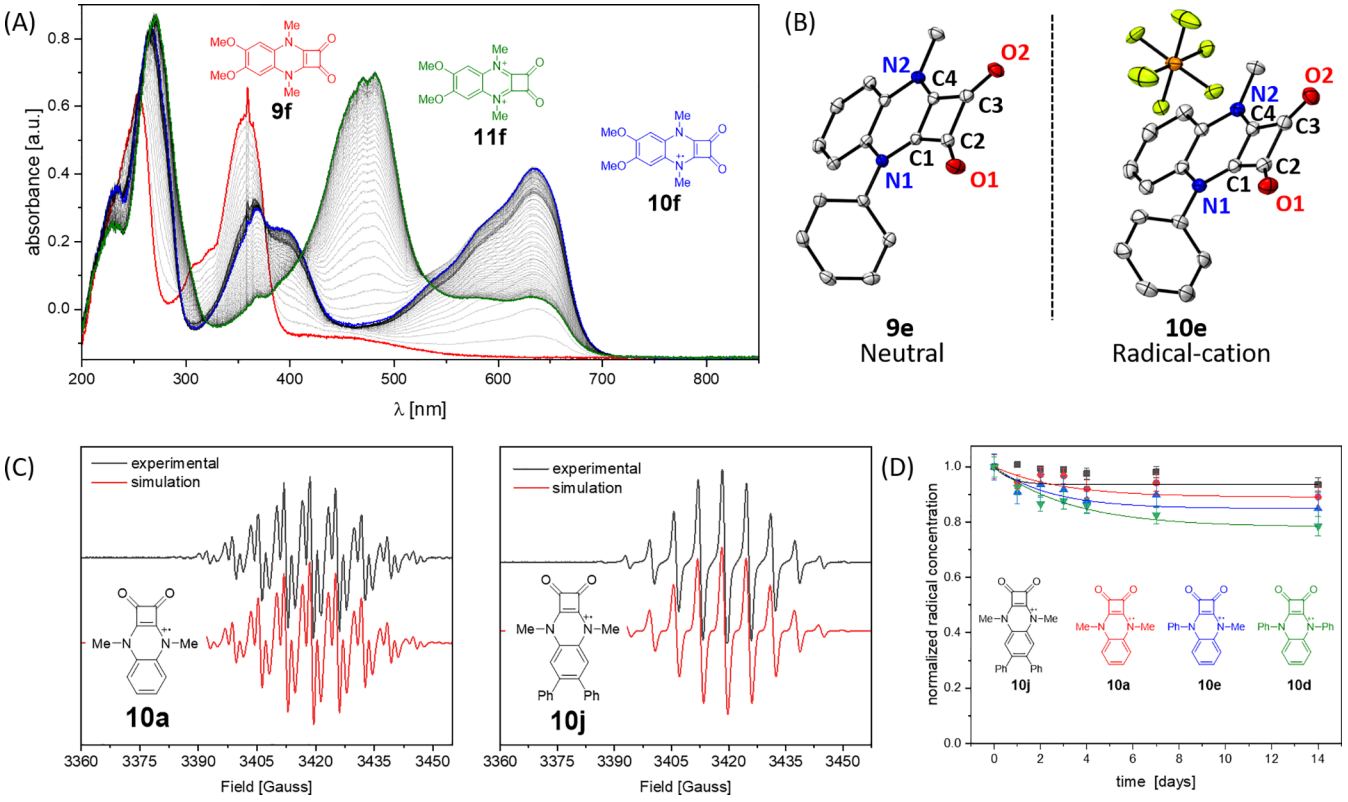

Figure 3. (A) Spectroelectrochemistry for the two-electron redox system **9f** → **10f** → **11f** and (B) X-ray solid-state structures of **9e** and **10e**. Thermal ellipsoids are shown with a 50% probability. Hydrogen atoms are omitted for clarity. Selected bond lengths and angles in [Å] and [°] **9e**: C1−C2 1.470(2), C2−C3 1.531(2), C3−C4 1.484(2), C1−C4 1.380(2), C2−O1 1.215(2), C3−O2 1.215(3), C1−N1 1.345(2), C1−C2−C3 87.4(1), C2−C3−C4 86.8(1); **10e**: C1−C2 1.494(2), C2−C3 1.570(2), C3−C4 1.496(2), C1−C4 1.378(2), C2−O1 1.197(2), C3−O2 1.195(3), C1−N1 1.336(2), C1−C2−C3 86.3(1), C2−C3−C4 86.3(1). (C) X-band EPR spectra of radical cations **10a** and **10l**; fitted (calculated) EPR parameter in [MHz]: 2xN 18.2 (19.4), 6xH 18.9 (18.7), 2xH 1.2 (1.8), 2xH 4.8 (4.4) (**10a**) and 2xN 18.3 (18.1), 6xH 17.3 (17.5) (**10l**). (D) Stability measurements of selected radical cations **10a**−**10b** and **10d**−**10e** by time-dependent UV−vis spectroscopy.

properties of the SQX small molecules prompted us to investigate the redox system in battery applications. Since it is known that small-molecular-weight redox systems may cause problems with undesired diffusion processes in the battery setup owing to their high solubility in organic electrolytes,[57] we aimed to develop a cathode redox system based on polymeric derivatives. We selected polymerizable units containing styrene linkers ($\mathbf{9^{M1}}$–$\mathbf{9^{M4}}$) with varying spacer elements. The styrene unit ($\mathbf{9^{M1}}$–$\mathbf{9^{M4}}$) was attached by alkylation of deprotonated **8a**–**8d** with 4-vinylbenzyl chloride (VBC) or 1-(5-bromopentyl)-4-vinylbenzene (BPV) (Scheme 4). The chain length was

Scheme 4. Synthesis of Redox-Active SQX Monomers ($\mathbf{9^{M1}}$–$\mathbf{9^{M4}}$) and SQX Polymers (P2–P4)

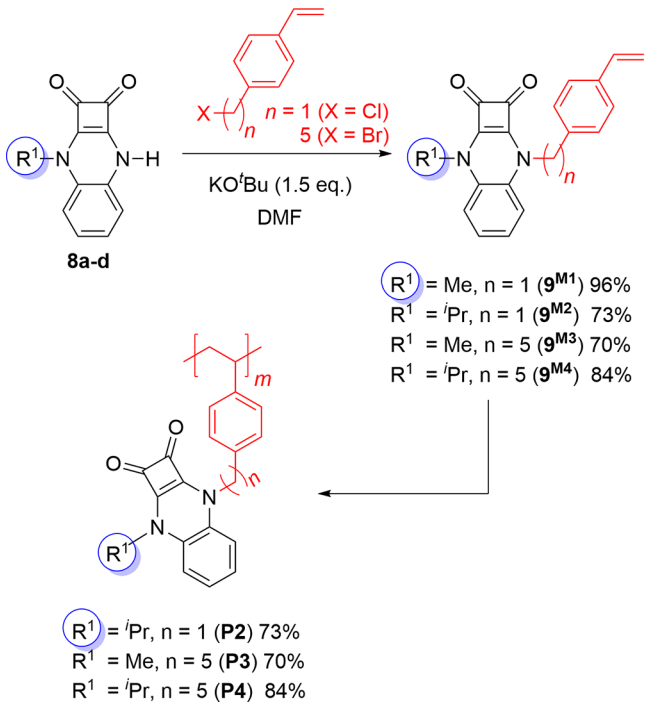

modified by varying one to five CH_2 units in order to investigate the chain mobility on polymerization conditions and physical properties. Additionally, the chain length should relate to the flexibility of the redox systems in the polymeric chain to favor or disfavor communication between the individual discrete redox sites. All monomers ($\mathbf{9^{M1}}$–$\mathbf{9^{M4}}$) exhibited exceptional high thermal stability with decomposition temperatures above 200 °C (see Figures S108–S111) and reversible oxidations in CH_2Cl_2 with values between 0.31 and 0.41 V vs $Fc^{0/+}$ (Figures S84–S88).

Reversible addition–fragmentation chain transfer (RAFT) polymerization was used as the preferred polymerization method to aim for good control over the degree of polymerization and dispersity of the polymers. In the case of $\mathbf{9^{M3}}$ and $\mathbf{9^{M4}}$, RAFT was too slow and could not provide the desired conversion. Therefore, free radical polymerization (FRP) was applied. Except for $\mathbf{9^{M1}}$, which could not be polymerized, presumably due to its limited solubility, all of the polymerizations proceeded overall with low yields (Table 1) yet provided sufficient amounts to afford further characterization. The low conversion of monomers in the polymerization (up to 49%) might be attributed to their limited solubility in DMF, despite the effort of RAFT polymerization to maintain lower molecular weights. For a summary of determined solubilities for selected SQX monomers, see the SI. Other solvents that were tested for polymerization included 1,4-dioxane, NMP, or toluene; however, they showed lower solvation of the SQX monomers. The conditions and results of the polymerizations are summarized in Table 1.

The respective polymers were characterized by NMR and size exclusion chromatography (SEC). The number-average molecular masses (M_n) of the polymers were determined by SEC in dimethylacetamide (DMAc) against PS or PMMA standards. It thus has to be noted that these M_n values were apparent molecular masses. The polymers with the highest M_n values (above 10,000 g mol^{-1}) were **P2** and **P4**, containing the *N*–*i*Pr substituents, while **P3** with N–Me featured smaller M_n values (M_n ~ 3,500 g mol^{-1}).

The thermal stabilities of obtained polymers **P2**–**P4** were examined via thermal gravimetric analysis (TGA). All SQX polymers exhibited remarkably high thermal stability in a nitrogen atmosphere [decomposition temperatures T_d = 290 °C (**P2**), 314 °C (**P3**) and 211 °C (**P4**)] (see Figures S112–S114). This exceptional thermal stability is essential to enable the processing of these polymers at elevated temperatures and increases the overall safety of the materials. The glass transition temperatures T_g (Table 1) were determined by differential scanning calorimetry (DSC). In the case of **P2**, the T_g value was remarkably high at 191 °C due to its rigid structure and bulky isopropyl group, limiting the chain mobility. The T_g values of **P3** and **P4** were slightly lower than the T_g of polystyrene (95 °C), which is ascribed to the higher mobility of the side groups due to the C5 linker, but higher than, for example, poly(4-hexylstyrene (−21 °C)).[58–60] Additionally, the effect of the SQX side groups on T_g was also shown as **P3**s methyl groups corresponded to the lower values and **P4**s isopropyl groups corresponded to the higher values, respectively. Next, the electrochemistry of polymers **P2**–**P4** was investigated. All exhibited a reversible oxidation event in CH_2Cl_2. $E_{1/2}$ (ca. 0.3 to 0.4 V vs $Fc^{0/+}$; and Figures S89–S91) slightly shifted by ca. 100 mV to lower potentials compared to the monomers $\mathbf{9^{M2}}$–$\mathbf{9^{M4}}$. The current intensity over the three cyclic sweeps remained nearly constant, indicating promising stability of the redox-active polymeric material.

Table 1. Polymerization Conditions and Properties of Polymers P2–P4[a]

monomer	polymer	time [h]	M_n [g mol^{-1}]	Đ	yield [%]	T_g [°C]	$E_{1/2}$ [V][c]
$\mathbf{9^{M2}}$	**P2**[a]	25	10,500	1.29	49	191.0	0.30
$\mathbf{9^{M3}}$	**P3**[b]	25	3,500	1.47	27	75.9	0.32
$\mathbf{9^{M4}}$	**P4**[b]	7	10,300	1.29	21	90.5	0.29

[a]The monomer concentration was set to 1 M, AIBN was used as an initiator, and anhydrous DMF was used as a solvent. All polymerizations were conducted at 80 °C except for **P2**, which was conducted at 90 °C. (a) RAFT polymerization: dibenzyl trithiocarbonate (DBTTC) was used as a chain transfer agent. (b) Free radical polymerization (FRP). (c) CVs in CH_2Cl_2 (0.1 M nBu$_4$PF$_6$) vs $Fc^{0/+}$.

Characterization as Li Battery Electrode Materials. Following these promising results, we fabricated battery-type electrodes to evaluate the redox activity in a state-of-the-art lithium battery electrolyte, i.e., 1 M $LiPF_6$ in a 1:1 weight mixture of ethylene carbonate (EC) and dimethyl carbonate (DMC), herein referred to as LP30. Since **P2** and **P4** feature an identical SQX core and a similar molecular weight, only differing in the chain lengths, these two polymers were selected as proof-of-concept model systems. The electrodes comprised the SQX polymer as the active material, conductive carbon (SC-65), graphene (G), and a binder (for details, see SI). These electrodes, hereinafter referred to as SQX-SC-65-G, were used as working electrodes in a three-electrode setup with a lithium-metal counter and reference electrode. The CV data are listed in Figure 5. The redox potential $E_{1/2}$ is about 3.69

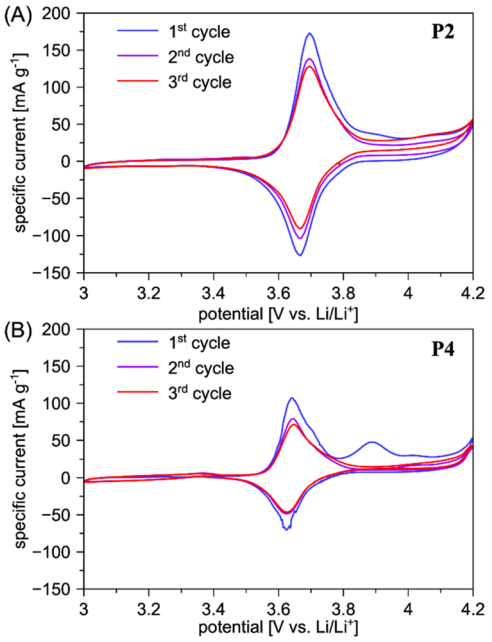

Figure 5. CV data of the SQX-SC-65-G electrodes comprising (A) **P2** and (B) **P4** as the active material in LP30 (scan rate: 0.1 mV s^{-1}) with 3.0 and 4.2 V as the reversing potentials.

and 3.63 V vs Li^+/Li for **P2** (Figure 5A) and **P4** (Figure 5B), respectively, which is very close to PTMA with 3.62 V (Figure S98) as the probably most investigated redox-active polymer. The slightly higher redox potential of **P2** is generally in line with the results obtained when electrochemistry is conducted in solution. Additionally, the longer linker chain length in **P4** might facilitate the $\pi-\pi$ interaction between the phenyl moieties of the redox-active molecule, which potentially stabilizes the oxidized molecule, thus lowering the oxidation potential slightly compared to **P2**. Overall, however, the CV data revealed a relatively stable current response (somewhat higher for **P2**), though it slightly decreased upon cycling. Moreover, the results showed an irreversible oxidation peak at about 3.9 V upon the first anodic sweep in both cases, indicating an irreversible second electron transfer initially. The effect of this irreversible oxidation process on the subsequent cycles, however, appeared to be little with regard to the rather reversible current response. Nonetheless, also, in view of the increase in current toward the anodic reversing potential, we decided to limit the anodic cutoff potential to 4.0 V for the subsequently conducted galvanostatic cycling.

The comparison of the first cycle dis-/charge profiles of **P2** (Figure 6A) and **P4** (Figure 6B) conducted at 0.05 A g^{-1}

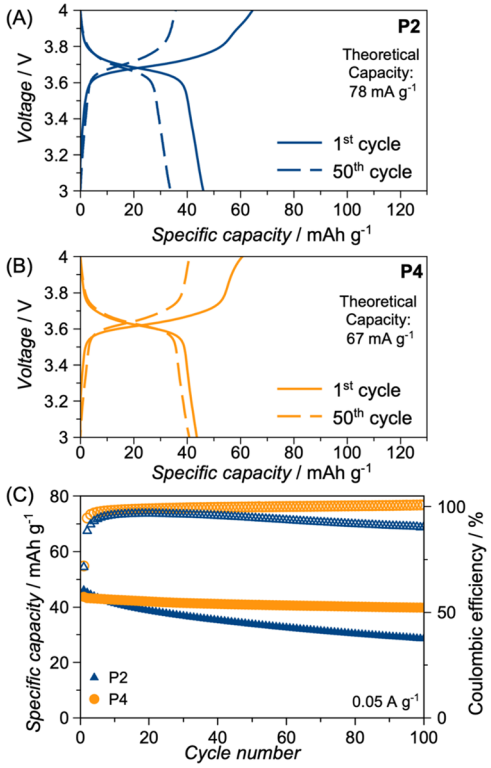

Figure 6. Galvanostatic cycling of the electrodes based on **P2** and **P4** with a lithium-metal counter electrode and LP30 as the electrolyte at 0.05 A g^{-1}: Comparison of the dis-/charge profiles for the 1st and 50th cycle for (A) **P2** and (B) **P4**. (C) Plot of the specific discharge capacity (solid data points) and Coulombic efficiency (hollow data points) vs the cycle number.

reveals a slightly higher specific discharge capacity for **P2** (46 vs 44 mAh g^{-1}). These values are somewhat lower than the theoretical capacities of 78 mAh g^{-1} (**P2**) and 67 mAh g^{-1} (**P4**). Even when the specific current was decreased from 0.05 to 0.01 A g^{-1}, the capacity remained lower than the theoretical values with 54 mAh g^{-1} for **P2** and 49 mAh g^{-1} for **P4** (Figure S99), suggesting that not all redox-active sites are accessible in the given setup. Nonetheless, the difference between the two SQX polymers is in line with the higher current intensity observed for **P2** via CV, as shown in Figure 5. When comparing the dis-/charge profiles of the first and the 50th cycle at 0.05 A g^{-1} (Figure 6A,6B), however, it becomes evident that the capacity retention is greater for **P4** (93 vs 73%). This is even more apparent from the plot of the specific capacity and Coulombic efficiency vs the cycle number, as displayed in Figure 6C. In both cases, the Coulombic efficiency rapidly increases initially but remains lower for **P2** with about 96% after 10 cycles, while it approaches 100% for **P4**. During the subsequent cycles, it remains very stable in the case of **P4**, while it continuously decreases for **P2** to about 95% after 50 cycles and only 90% after 100 cycles. This results in a continuous capacity fading for **P2** and a high cycling stability for **P4** with a capacity retention of 91% after 100 cycles (vs 61% for **P2** after 100 cycles; also see Figure S100).

The superior cycling stability of **P4** might be related to the aforementioned easier $\pi-\pi$ interaction, stabilizing the oxidized

state of the molecule and ensuring the maintenance of the electrochemical activity. The comparison of the rate capability of **P2** and **P4** (Figure 7A) revealed a substantially greater

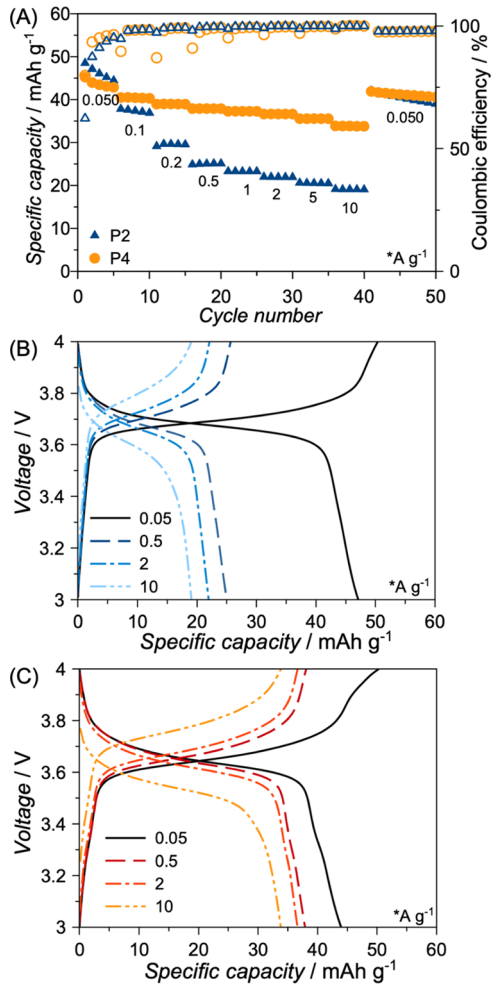

Figure 7. Galvanostatic cycling of the electrodes based on **P2** and **P4** with a lithium-metal counter electrode and LP30 as an electrolyte at varying specific currents, ranging from 0.05 to 10 A g^{-1}: the plot of the specific discharge capacity (solid data points) and Coulombic efficiency (hollow data points) vs the cycle number (A) and selected dis-/charge profiles at 0.05, 0.5, 2, and 10 A g^{-1} for **P2** (B) and **P4** (C).

performance for **P4** with only a relatively minor decrease in capacity even at a specific current of 10 A g^{-1}, at which still 33 mAh g^{-1} was obtained. Differently, the capacity of **P2** dropped to only 19 mAh g^{-1} at the same specific current. The comparison of the corresponding dis-/charge profiles of **P2** (Figure 7B) and **P4** (Figure 7C) indicates that this is only partially due to a higher polarization in the case of **P2**, while there is a significant shortening of the voltage plateau, suggesting limited accessibility of the redox-active sites. This might be related to a different organization of the two polymers at the macroscopic level,[61] which will have to be investigated in more detail in the future.

Nonetheless, the achievable specific capacity and the rate capability of **P4** are very comparable to other organic cathode materials with a redox potential of well above 3 V as, for instance, phenothiazine derivatives,[62,63] highlighting the general suitability of this material class for application in polymer batteries.

CONCLUSIONS

This study introduced a new redox-active moiety, i.e., squaric acid amides (SQAs), to the field of energy storage. In the first part, we identified that the low stability of 1,2-SQA, 1,3-SQA, and SSQA radical cations hampers the applications of SQA in energy storage. Upon embedding the SQA system into a quinoxaline heterocycle (SQX), highly robust radical cations could be characterized, including EPR spectroscopy and X-ray diffraction. Such radical cations show very high stabilities, even in the presence of air, over several days/weeks, which could be demonstrated by time-dependent UV−vis as well as charge/discharge experiments. Subsequently, the first SQX-functionalized polymers were reported, which were evaluated as novel positive electrode active materials in polymer batteries. Three styrene-based monomers were successfully polymerized and structurally characterized. All SQX polymers exhibited high redox potentials and reversible redox reactions in solution. In combination with lithium-metal counter electrodes and state-of-the-art lithium battery electrolytes, very stable cycling for the one-electron oxidation was observed for more than 100 cycles with a capacity retention of 91%, accompanied by an excellent rate capability.

Our work demonstrates a proof-of-concept that squaric acid amide-derived molecules such as SQXs are worthy of consideration as novel organic cathode materials for energy storage and encourages further applications of this unique redox system class. Future work will address and optimize aspects such as the solubility and the impact of the electrolyte as well as the size and structural compositions of the SQX polymers. Besides, the theoretical and eventually obtained capacity still needs to be increased. In this regard, one possible pathway toward higher capacities is the stabilization of the second electron transfer. As a result, given the fact that the SQX systems are highly modular and rapid to synthesize from cheap commercially available starting materials, this molecule class bears great potential and opens up a new structural space to be exploited in the context of redox-active organic materials.

AUTHOR INFORMATION

Corresponding Authors

Dominic Bresser − *Helmholtz Institute Ulm (HIU), D-89081 Ulm, Germany; Karlsruhe Institute of Technology (KIT), D-76021 Karlsruhe, Germany;* orcid.org/0000-0001-6429-6048; Email: dominic.bresser@kit.edu

Patrick Théato − *Institute for Chemical Technology and Polymer Chemistry (ITCP), Karlsruhe Institute of Technology (KIT), D-76131 Karlsruhe, Germany; Soft Matter Synthesis Laboratory, Institute for Biological Interfaces III, D-76344 Eggenstein-Leopoldshafen, Germany;* orcid.org/0000-0002-4562-9254; Email: patrick.theato@kit.edu

Max M. Hansmann − *Faculty of Chemistry and Chemical Biology (CCB), Technical University Dortmund, D-44227 Dortmund, Germany;* orcid.org/0000-0003-3107-1445; Email: max.hansmann@tu-dortmund.de

Authors

Marcel E. Baumert − *Faculty of Chemistry and Chemical Biology (CCB), Technical University Dortmund, D-44227 Dortmund, Germany*

Victoria Le − *Institute for Chemical Technology and Polymer Chemistry (ITCP), Karlsruhe Institute of Technology (KIT), D-76131 Karlsruhe, Germany*

Po-Hua Su − *Helmholtz Institute Ulm (HIU), D-89081 Ulm, Germany; Karlsruhe Institute of Technology (KIT), D-76021 Karlsruhe, Germany*

Yosuke Akae − *Institute for Chemical Technology and Polymer Chemistry (ITCP), Karlsruhe Institute of Technology (KIT), D-76131 Karlsruhe, Germany; Research Fellow of Japan Society for the Promotion of Science, 102-0083 Tokyo, Japan*

Author Contributions

M.E.B., V.L. and P.-H. S. contributed equally to this work. All authors have given approval to the final version of the manuscript.

Funding

This work was funded by the German Research Foundation through funding within the priority program SPP 2248 “Polymer-Based Batteries” (441254245; project numbers HA 8832/2-1; TH 1104/18-1; BR 5752/4-1).

Notes

The authors declare no competing financial interest.

ACKNOWLEDGMENTS

Patrick Antoni and Taichi Koike (TUD) are thanked for the measurement of the X-ray solid-state structures, and Lars Hebenbrock, Nicole Winterholler, and Seyma Ceylan (TUD) for synthetic help. Experimental support [NMR (TUD): DFG project 452669591] and computational resources were provided by LiDO3, the high-performance computing facility at TU Dortmund (DFG project 271512359).

REFERENCES

(1) Chen, Y.; Kang, Y.; Zhao, Y.; Wang, L.; Liu, J.; Li, Y.; Liang, Z.; He, X.; Li, X.; Tavajohi, N.; Li, B. A review of lithium-ion battery safety concerns: The issues, strategies, and testing standards. *J. Energy Chem.* **2021**, *59*, 83−99.

(2) Mayyas, A.; Steward, D.; Mann, M. The case for recycling: Overview and challenges in the material supply chain for automotive li-ion batteries. *Sustainable Mater. Technol.* **2019**, *19*, No. e00087.

(3) Usai, L.; Lamb, J. J.; Hertwich, E.; Burheim, O. S.; Strømman, A. H. Analysis of the Li-ion battery industry in light of the global transition to electric passenger light duty vehicles until 2050. *Environ. Res.: Infrastruct. Sustain.* **2022**, *2*, 11002.

(4) Armand, M.; Tarascon, J.-M. Building better batteries. *Nature* **2008**, *451*, 652−657.

(5) Schon, T. B.; McAllister, B. T.; Li, P.-F.; Seferos, D. S. The rise of organic electrode materials for energy storage. *Chem. Soc. Rev.* **2016**, *45*, 6345−6404.

(6) Hager, M. D.; Esser, B.; Feng, X.; Schuhmann, W.; Theato, P.; Schubert, U. S. Polymer-Based Batteries-Flexible and Thin Energy Storage Systems. *Adv. Mater.* **2020**, *32*, No. e2000587.

(7) Muench, S.; Wild, A.; Friebe, C.; Häupler, B.; Janoschka, T.; Schubert, U. S. Polymer-Based Organic Batteries. *Chem. Rev.* **2016**, *116*, 9438.

(8) Esser, B. Redox Polymers as Electrode-Active Materials for Batteries. *Org. Mater.* **2019**, *01*, 063−070.

(9) Cao, X.; Liu, J.; Zhu, L.; Xie, L. Polymer Electrode Materials for High-Performance Lithium/Sodium-Ion Batteries: A Review. *Energy Technol.* **2019**, *7*, No. 1800759.

(10) Xu, S.; Dai, H.; Zhu, S.; Wu, Y.; Sun, M.; Chen, Y.; Fan, K.; Zhang, C.; Wang, C.; Hu, W. A branched dihydrophenazine-based polymer as a cathode material to achieve dual-ion batteries with high energy and power density. *eScience* **2021**, *1*, 60−68.

(11) Suga, T.; Sugita, S.; Ohshiro, H.; Oyaizu, K.; Nishide, H. p- and n-Type bipolar redox-active radical polymer: Toward totally organic polymer-based rechargeable devices with variable configuration. *Adv. Mater.* **2011**, *23*, 751−754.

(12) Goujon, N.; Casado, N.; Patil, N.; Marcilla, R.; Mecerreyes, D. Organic batteries based on just redox polymers. *Prog. Polym. Sci.* **2021**, *122*, No. 101449.

(13) Hatakeyama-Sato, K.; Tezuka, T.; Ichinoi, R.; Matsumono, S.; Sadakuni, K.; Oyaizu, K. Metal-Free, Solid-State, Paper like Rechargeable Batteries Consisting of Redox-Active Polyethers. *ChemSusChem* **2020**, *13*, 2443−2448.

(14) Kye, H.; Kang, Y.; Jang, D.; Kwon, J. E.; Kim, B.-G. p-Type Redox-Active Organic Electrode Materials for Next-Generation Rechargeable Batteries. *Adv. Energy Sustainable Res.* **2022**, *3*, No. 2200030.

(15) Poizot, P.; Gaubicher, J.; Renault, S.; Dubois, L.; Liang, Y.; Yao, Y. Opportunities and Challenges for Organic Electrodes in Electrochemical Energy Storage. *Chem. Rev.* **2020**, *120*, 6490−6557.

(16) Kwon, G.; Lee, S.; Hwang, J.; Shim, H.-S.; Lee, B.; Lee, M. H.; Ko, Y.; Jung, S.-K.; Ku, K.; Hong, J.; Kang, K. Multi-redox Molecule for High-Energy Redox Flow Batteries. *Joule* **2018**, *2*, 1771−1782.

(17) Winsberg, J.; Stolze, C.; Schwenke, A.; Muench, S.; Hager, M. D.; Schubert, U. S. Aqueous 2,2,6,6-Tetramethylpiperidine-N-Oxyl Catholytes for a High-Capacity and High Current Density Oxygen-Insensitive Hybrid-Flow Battery. *ACS Energy Lett.* **2017**, *2*, 411−416.

(18) Liu, Y.; Goulet, M.-A.; Tong, L.; Liu, Y.; Ji, Y.; Wu, L.; Gordon, R. G.; Aziz, M. J.; Yang, Z.; Xu, T. A Long-Lifetime All-Organic Aqueous Flow Battery Utilizing TMAP-TEMPO Radical. *Chem.* **2019**, *5*, 1861−1870.

(19) Hu, B.; Hu, M.; Luo, J.; Liu, T. L. A Stable, Low Permeable TEMPO Catholyte for Aqueous Total Organic Redox Flow Batteries. *Adv. Energy Mater.* **2021**, *12*, No. 2102577.

(20) Milshtein, J. D.; Kaur, A. P.; Casselman, M. D.; Kowalski, J. A.; Modekrutti, S.; Zhang, P. L.; Harsha Attanayake, N.; Elliott, C. F.; Parkin, S. R.; Risko, C.; Brushett, F. R.; Odom, S. A. High current density, long duration cycling of soluble organic active species for non-aqueous redox flow batteries†. *Energy Environ. Sci.* **2016**, *9*, 3531−3543.

(21) Kowalski, J. A.; Casselman, M. D.; Kaur, A. P.; Milshtein, J. D.; Elliott, C. F.; Modekrutti, S.; Attanayake, N. H.; Zhang, N.; Parkin, S. R.; Risko, C.; Brushett, F. R.; Odom, S. A. A Stable Two-Electron-Donating Phenothiazine for Application in Nonaqueous Redox Flow Batteries. *J. Mater. Chem. A* **2017**, *5*, 24371−24379.

(22) Walser-Kuntz, R.; Yan, Y.; Sigman, M. S.; Sanford, M. S. A Physical Organic Chemistry Approach to Developing Cyclopropenium-Based Energy Storage Materials for Redox Flow Batteries. *Acc. Chem. Res.* **2023**, *56*, 1239−1250.

(23) Sevov, C. S.; Samaroo, S. K.; Sanford, M. S. Cyclopropenium Salts as Cyclable, High-Potential Catholytes in Nonaqueous Media. *Adv. Energy Mater.* **2016**, *7*, No. 1602027.
(24) Yan, Y.; Robinson, S. G.; Sigman, M. S.; Sanford, M. S. Mechanism-Based Design of a High-Potential Catholyte Enables a 3.2 V All-Organic Nonaqueous Redox Flow Battery. *J. Am. Chem. Soc.* **2019**, *141*, 15301−15306.
(25) Robinson, S. G.; Yan, Y.; Hendriks, K. H.; Sanford, M. S.; Sigman, M. S. Developing a Predictive Solubility Model for Monomeric and Oligomeric Cyclopropenium-Based Flow Battery Catholytes. *J. Am. Chem. Soc.* **2019**, *141*, 10171−10176.
(26) Buhrmester, C.; Chen, J.; Moshurchak, L.; Jiang, J.; Wang, R. L.; Dahn, J. R. Studies of Aromatic Redox Shuttle Additives for LiFePO[Sub 4]-Based Li-Ion Cells. *J. Electrochem. Soc.* **2005**, *152*, A2390.
(27) Zhang, L.; Zhang, Z.; Redfern, P. C.; Curtiss, L. A.; Amine, K. Molecular Engineering towards Safer Lithium-Ion Batteries: A Highly Stable and Compatible Redox Shuttle for Overcharge Protection. *Energy Environ. Sci.* **2012**, *5*, 8204.
(28) Zhang, J.; Shkrob, I. A.; Assary, R. S.; Tung, S. on.; Silcox, B.; Curtiss, L. A.; Thompson, L.; Zhang, L. Toward Improved Catholyte Materials for Redox Flow Batteries: What Controls Chemical Stability of Persistent Radical Cations? *J. Phys. Chem. C* **2017**, *121*, 23347−23358.
(29) Janoschka, T.; Hager, M. D.; Schubert, U. S. Powering up the future: radical polymers for battery applications. *Adv. Mater.* **2012**, *24*, 6397−6409.
(30) Nakahara, K.; Iwasa, S.; Satoh, M.; Morioka, Y.; Iriyama, J.; Suguro, M.; Hasegawa, E. Rechargeable batteries with organic radical cathodes. *Chem. Phys. Lett.* **2002**, *359*, 351−354.
(31) Nishide, H.; Koshika, K.; Oyaizu, K. Environmentally benign batteries based on organic radical polymers. *Pure Appl. Chem.* **2009**, *81*, 1961−1970.
(32) Suga, T.; Ohshiro, H.; Sugita, S.; Oyaizu, K.; Nishide, H. Emerging N-Type Redox-Active Radical Polymer for a Totally Organic Polymer-Based Rechargeable Battery. *Adv. Mater.* **2009**, *21*, 1627−1630.
(33) Gracia, R.; Mecerreyes, D. Polymers with redox properties: materials for batteries, biosensors and more. *Polym. Chem.* **2013**, *4*, 2206−2214.
(34) Niu, Z.; Wu, H.; Liu, L.; Dai, G.; Xiong, S.; Zhao, Y.; Zhang, X. Chain Rigidity Modification to Promote the Electrochemical Performance of Polymeric Battery Electrode Materials. *J. Mater. Chem. A* **2019**, *7*, 10581−10588.
(35) Gannett, C. N.; Peterson, B. M.; Shen, L.; Seok, J.; Fors, B. P.; Abruña, H. D. Cross-linking Effects on Performance Metrics of Phenazine-Based Polymer Cathodes. *ChemSusChem* **2020**, *13*, 2428−2435.
(36) Gannett, C. N.; Peterson, B. M.; Melecio-Zambrano, L.; Trainor, C. Q.; Fors, B. P.; Abruña, H. D. Performance Optimization and Fast Rate Capabilities of Novel Polymer Cathode Materials through Balanced Electronic and Ionic Transport. *J. Mater. Chem. A* **2021**, *9*, 5657−5663.
(37) Studer, G.; Schmidt, A.; Büttner, J.; Schmidt, M.; Fischer, A.; Krossing, I.; Esser, B. On a high-capacity aluminium battery with a two-electron phenothiazine redox polymer as positive electrode. *Energy Environ. Sci.* **2023**, *16*, 3760.
(38) Wessling, R.; Andres, R. D.; Morhenn, I.; Acker, P.; Maftuhin, W.; Walter, M.; Würfel, U.; Esser, B. Phenothiazine-Based Donor−Acceptor Polymers as Multifunctional Materials for Charge Storage and Solar Energy Conversion. *Macromol. Rapid Commun.* **2022**, No. 2200699.
(39) Otteny, F.; Perner, V.; Wassy, D.; Kolek, M.; Bieker, P.; Winter, M.; Esser, B. Poly(vinylphenoxazine) as Fast-Charging Cathode Material for Organic Batteries. *ACS Sustainable Chem. Eng.* **2020**, *8*, 238−247.
(40) Nesvadba, P.; Folger, L. B.; Maire, P.; Novák, P. Synthesis of a Polymeric 2,5-Di-t-Butyl-1,4-Dialkoxybenzene and Its Evaluation as a Novel Cathode Material. *Synth. Met.* **2011**, *161*, 259−262.
(41) Montoto, E. C.; Cao, Y.; Hernández-Burgos, K.; Sevov, C. S.; Braten, M. N.; Helms, B. A.; Moore, J. S.; Rodríguez-López, J. Effect of the Backbone Tether on the Electrochemical Properties of Soluble Cyclopropenium Redox-Active Polymers. *Macromolecules* **2018**, *51*, 3539−3546.
(42) Malerich, J. P.; Hagihara, K.; Rawal, V. H. Chiral Squaramide Derivatives are Excellent Hydrogen Bond Donor Catalysts. *J. Am. Chem. Soc.* **2008**, *130*, 14416−14417.
(43) Rostami, A.; Colin, A.; Li, X. Y.; Chudzinski, M. G.; Lough, A. J.; Taylor, M. S. N,N′-Diarylsquaramides: General, High-Yielding Synthesis and Applications in Colorimetric Anion Sensing. *J. Org. Chem.* **2010**, *75*, 3983−3992.
(44) Gilbert, A. M.; Antane, M. M.; Argentieri, T. M.; Butera, J. A.; Francisco, G. D.; Freeden, C.; Gundersen, E. G.; Graceffa, R. F.; Herbst, D.; Hirth, B. H.; Lennox, J. R.; McFarlane, G.; Norton, N. W.; Quagliato, D.; Sheldon, J. H.; Warga, D.; Wojdan, A.; Woods, M. Design and SAR of Novel Potassium Channel Openers Targeted for Urge Urinary Incontinence. 2. Selective and Potent Benzylamino Cyclobutenediones. *J. Med. Chem.* **2000**, *43*, 1203−1214.
(45) Hünig, S.; Pütter, H. Elektrochemisches Verhalten von Quadratsäure-amiden. *Chem. Ber.* **1977**, *110*, 2524−2531.
(46) Ehrhardt, H.; Hünig, S.; Pütter, H. Amide und Thioamide der Quadratsäure: Synthese und Reaktionen. *Chem. Ber.* **1977**, *110*, 2506−2523.
(47) Deuchert, K.; Hünig, S. Multistage Organic Redox Systems—A General Structural Principle. *Angew. Chem., Int. Ed.* **1978**, *17*, 875−886.
(48) Reference 43 indicated the necessity of $Zn(OTf)_2$ as Lewis-acid for the generation of 1,2-SQA molecules, which was under our reaction conditions not required.
(49) Hünig, S.; Pütter, H. Neue Wege zu Quadratsäure-1,3-diamiden. *Angew. Chem.* **1972**, *84*, 480−481.
(50) Schmidt, A. H.; Schmitt, G.; Diedrich, H. Oxokohlenstoffe und verwandte Verbindungen; 15. Mitteilung. Meerwein-Arylierung von Semiquadratsäure und Semiquadratsäureamiden. Eine allgemeine Darstellungsmethode von 3-Aryl-4-hydroxy- und 3-Amino-4-aryl-3-cyclobuten-1,2-dionen. *Synthesis* **1990**, *7*, 579−582.
(51) Ohsedo, Y.; Miyamoto, M.; Tanaka, A.; Watanabe, H. Synthesis and electrochemical properties of symmetric squarylium dyes containing diarylamine. *Dyes Pigm.* **2014**, *101*, 261−269.
(52) Small, D.; Zaitsev, V.; Jung, Y.; Rosohka, S. V.; Head-Gordon, M.; Kochi, J. K. Intermolecular π-to-π Bonding between Stacked Aromatic Dyads. Experimental and Theoretical Binding Energies and Near-IR Optical Transitions for Phenalenyl Radical/Radical versus Radical/Cation Dimerizations. *J. Am. Chem. Soc.* **2004**, *126*, 13850−13858.
(53) For N-H substitution an even older synthesis is described, see: (a) Skujins, S.; Webb, G. A. Synthesis of cyclobuta[b]quinoxalines. *Chem. Commun.* **1968**, *11*, 598. (b) Ried, W.; Kunstmann, W. Reaktionen mit Cyclobutendionen, VI. Notiz zur Synthese der 1.2.3.8-Tetrahydro-cyclobuta[b]chinoxalin-dionen-(1.2). *Chem. Ber.* **1969**, *102*, 1439−1440.
(54) Schmidt, W.; Steckhan, E. Über organische Elektronenüberträgersysteme, I. Elektrochemische und spektroskopische Untersuchung bromsubstituierter Triarylamin-Redoxsysteme. *Chem. Ber.* **1980**, *113*, 577−585, DOI: 10.1002/cber.19801130215.
(55) Deposition numbers 2289869 (**2b**), 2289870 (**4b**), 2289871 (**9e**), 2289872 (for **10e**), 2289873 (for **10i**) contain the supplementary crystallographic data for this paper. These data are provided free of charge by the joint Cambridge Crystallographic Data Centre and Fachinformationszentrum Karlsruhe.
(56) Hioe, J.; Šakić, D.; Vrček, V.; Zipse, H. The stability of nitrogen-centered radicals. *Org. Biomol. Chem.* **2015**, *13*, 157−169.
(57) Hendriks, K. H.; Robinson, S. G.; Braten, M. N.; Sevov, C. S.; Helms, B. A.; Sigman, M. S.; Minteer, S. D.; Sanford, M. S. High-Performance Oligomeric Catholytes for Effective Macromolecular Separation in Nonaqueous Redox Flow Batteries. *ACS Cent. Sci.* **2018**, *4*, 189−196.

(58) Rieger, J. The glass transition temperature of polystyrene. *J. Therm. Anal.* **1996**, *46*, 965−972.
(59) Yu, X.; Huang, X. A quantitative relationship between Tgs and chain segment structures of polystyrenes. *Polimeros* **2017**, *27*, 68−74.
(60) Gaur, U.; Lau, S.; Wunderlich, B. B.; Wunderlich, B. Heat Capacity and Other Thermodynamic Properties of Linear Macromolecules VI. Acrylic Polymers. *J. Phys. Chem. Ref. Data* **1982**, *11*, 1065−1089.
(61) Ademmer, M.; Su, P.-H.; Dodell, L.; Asenbauer, J.; Osenberg, M.; Hilger, A.; Chang, J.-K.; Manke, I.; Neumann, M.; Schmidt, V.; Bresser, D. Unveiling the Impact of Cross-Linking Redox-Active Polymers on Their Electrochemical Behavior by 3D Imaging and Statistical Micro-structure Analysis. *J. Phys. Chem. C* **2023**, DOI: 10.1021/acs.jpcc.3c04162.
(62) Kolek, M.; Otteny, F.; Schmidt, P.; Mück-Lichtenfeld, C.; Einholz, C.; Becking, J.; Schleicher, E.; Winter, M.; Bieker, P.; Esser, B. Ultra-high cycling stability of poly (vinylphenothiazine) as a battery cathode material resulting from $\pi-\pi$ interactions. *Energy Environ. Sci.* **2017**, *10*, 2334−2341.
(63) Dai, G.; Liu, Y.; Niu, Z.; He, P.; Zhao, Y.; Zhang, X.; Zhou, H. The design of quaternary nitrogen redox center for high-performance organic battery materials. *Matter* **2019**, *1*, 945−958.